# Coseismic fault model of the 2008 Iwate-Miyagi Nairiku earthquake deduced by a dense GPS network

Yusaku Ohta, Mako Ohzono, Satoshi Miura, Takeshi Iinuma, Kenji Tachibana, Kota Takatsuka, Kayo Miyao, Toshiya Sato, and Norihito Umino

*Research Center for Prediction of Earthquakes and Volcanic Eruptions, Graduate School of Science, Tohoku University, Sendai 980-8578, Japan*

(Received August 18, 2008; Revised September 2, 2008; Accepted September 5, 2008; Online published December 10, 2008)

A large earthquake of $M_j$ 7.2 occurred on June 14, 2008, beneath the border between Iwate and Miyagi prefectures in northeastern Japan. We propose a simple rectangular fault model based on a dense GPS network, including continuous GPS sites run by four agencies, to describe the coseismic deformation. The coseismic displacements are estimated by kinematic PPP (precise point positioning) analysis. Near the hypocenter, co-located independent instruments (integrated accelerogram and kinematic PPP) measure the same large displacement caused by the mainshock. The fault model explains the observations well and reproduces the observed complex spatial pattern, especially around the northern part of the focal area, which is the focus of a debate on whether or not the coseismic slip occurred on the Dedana fault system. Our results show that no major slip on the Dedana fault system occurred. The estimated amount of moment release was equivalent to $M_w$ 6.9, and the maximum slip reached 3.5 m on the southern sub-fault.

**Key words:** 2008 Iwate-Miyagi Nairiku earthquake, kinematic GPS, coseismic fault model.

## 1. Introduction

The 2008 Iwate-Miyagi Nairiku (inland) earthquake (hereafter IMEQ) occurred beneath the border between the Iwate and Miyagi prefectures in northeastern (NE) Japan at 08:43 JST, 14 June 2008. The focal mechanism proposed by the National Research Institute for Earth Science and Disaster Prevention (NIED) suggests that a reverse fault motion occurred with a west-northwest (W-NW) to east-southeast (E-SE) compression axis (Fig. 1). Miura *et al.* (2002, 2004) found the existence of a notable strain concentration zone with an E-W contraction along the Ou backbone range (OBR), where the Volcanic Front runs through, using continuous GPS measurements. This E-W contraction zone also shows a higher shallow earthquake activity, with most activity occurring in the upper crust, similar to the focal areas of large inland earthquakes, such as the 1896 Riku-u earthquake ($M$ 7.2; see Matsuda *et al.*, 1980), the 1970 Southeastern Akita earthquake ($M$ 6.2; Hasegawa *et al.*, 1974, 1975), Shizukuishi earthquake ($M$ 6.1; Umino *et al.*, 1998; Miura *et al.*, 2000), and so on. The main shock of the IMEQ and its many aftershocks were located within this tectonically active region. Furthermore, an active fault, denoted the Kitakami-Teichi Seien Fault Zone (KTSFZ) exists close to the IMEQ focal area. The KTSFZ is composed of several small active faults and the southernmost fault is called the Dedana Fault (DF). In this paper, we describe the coseismic displacement field observed with our dense GPS network and GEONET sites, and we discuss the characteristics of the coseismic fault model and its relationship to the fault systems around the rupture area.



## 2. Data and Analysis

GEONET, a nationwide GPS network composed of more than 1,200 stations, was established by the Geographical Survey Institute (GSI) (e.g. Hatanaka, 2003). There are not enough GEONET sites near the OBR because of the area's mountainous topography. For moderately sized inland earthquakes with magnitudes between 6 and 7, the spatial density of GEONET is insufficient for determining detailed coseismic fault motion. Between 1994 and 2003, Miura *et al.* (2006) established 13 new continuous GPS stations in Miyagi and Iwate prefectures to complement GEONET and improve sampling resolution of the interplate slip expected during the predicted Miyagi-oki earthquake. In addition, in October 2007, the Japan Nuclear Energy Safety Organization (JNES) established a new continuous GPS array along an E-W traverse running through the northern end of the IMEQ focal area and across the DF (Fig. 1) with the aim of studying methodology for improving the seismic safety of nuclear installations through seismic risk evaluation. The National Astronomical Observatory of Japan (NAO) also operated three GPS sites in Mizusawa, to the east of KTSFZ on the same traverse as JNES stations.

We have aggregated the data from the continuous GPS stations from four different institutions, including Tohoku University (TU), GSI, JNES, and NAO. The GPS data were sampled at 1-s, 30-s, or 1-min intervals, depending on the receiver type and telemetry system. Dual-frequency receivers were deployed at all stations. Data from the TU and JNES networks are transmitted on a public telephone line or broadband Internet every day.

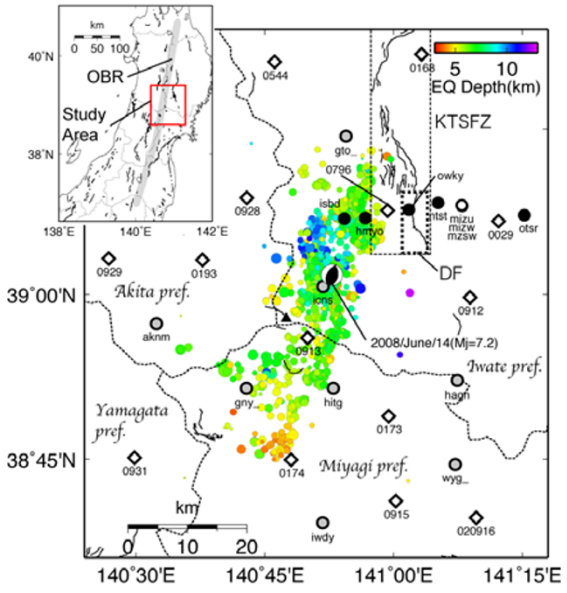


Fig. 1. Location map of GPS sites around focal area. OBR denotes the Ou Backbone Range. Red rectangular represents the study area. The aftershocks measured by the group for the aftershock observations of the Iwate-Miyagi Nairiku earthquake in 2008 (GIMNE2008) between 14–17 and 20 June 2008 are shown by colored circles. The sizes of each circle are proportional to the magnitude of the earthquake. Gray, black, and open circles denote GPS sites operated by Tohoku University, JNES, and NAO, respectively. Open diamonds represent GEONET GPS sites. The earthquake mechanism is determined by NIED. Black triangle denotes Mt. Kurikoma. The thin dashed rectangle and the thick rectangle indicate the Kitakami-Teichi Seien Fault Zone (KTSFZ) and the Dedana Fault (DF), respectively. Thin dashed lines denote prefecture borders.

Precise point positioning (PPP; Zumberge *et al.*, 1997) kinematic analysis coupled with GPS measurement has recently become one of the preferred methods for observing dynamic crustal deformations (e.g. Kouba, 2003; Takasu, 2006). We used GPSTools version 0.6.3. (Takasu and Kasai, 2005), which is a GPS processing suite developed in Japan, to process the data using the kinematic PPP strategy. The PPP method uses data such as precise ephemeredes, GPS satellite clock corrections, and earth rotation parameters provided by various analysis centers, such as International GNSS Service (IGS), to precisely estimate the site coordinates without any reference sites. We processed 14 and 15 June for kinematic PPP solutions by dual frequency analysis. The time-dependent unknown parameters (three-component coordinate, zenith tropospheric delay, and station clock) are estimated using an extended Kalman filter (forward/backward). Carrier phase ambiguities were not resolved. The GPS receiver coordinates were estimated using a strictly constrained random walk stochastic model (random walk sigma is 10 mm $s^{-1/2}$) every 5 min (required because data from each GPS site were sampled at different intervals). Most kinematic earthquake studies adopted for the independent (white noise) stochastic model because of these studies seek unbiased dynamic displacements, such as seismic wave passing (Larson *et al.*, 2003; Ohta *et al.*, 2006). In this study, our aim was to detect the coseismic step. Therefore, some level of correlation between the positions is negligible. The strictly constrained random walk model also produces a low-scatter time series. The N-S, E-W, and up-down component for the root mean square (rms) error for five epochs of all GPS stations before the earthquake are 5.2, 4.3, and 10.4 mm, respectively. In this study, we adopted the IGS final products (Dow *et al.*, 2005). The IGS final orbits and clocks are provided in the IGS05 reference frame. Consequently, the position solutions are also defined within the IGS05 reference frame. Following kinematic PPP processing, we chose GEONET site 950154 (Iwasaki), located about 200 km NW of the epicenter (not shown in Fig. 1), as the reference site to remove the satellite origin's common-mode noise.

## 3. Results and Discussion

### 3.1 Coseismic displacement detection by kinematic GPS analysis

Kinematic or sub-daily GPS processing can detect exact co-seismic displacements, whereas daily analyses can be contaminated by a mixture of true coseismic and short-term postseismic signals (Miyazaki and Larson, 2008). Figure 2 shows an example of the kinematic GPS coordinate time series with a 5-min interval at the ICNS station located 2.5 km southwest of the epicenter (see also Fig. 1), which is the nearest GPS site to the hypocenter. It is clear that the kinematic PPP strategy successfully detects the large coseismic step of the mainshock. We defined the coseismic displacement as the difference averaged over 25 min (five epochs) before and after the mainshock. If any GPS station experienced a power outage after the main shock (shortest power outage was for 2 h, and the longest power outage reached 3 days), we defined the coseismic displacement as the difference averaged over 25 min before and after the power outage. We summarize the coseismic displacements in Table 1 for all GPS sites used in this study and show the coseismic displacements for nearby GPS stations in Fig. 3.

Near the hypocenter, co-located independent instruments measure the same displacements. As shown in Fig. 2, the ICNS station clearly undergoes horizontal and vertical displacements, with magnitudes of 44 cm (east), 34 cm (north), and 156 cm (up). NIED (2008) also reported co-

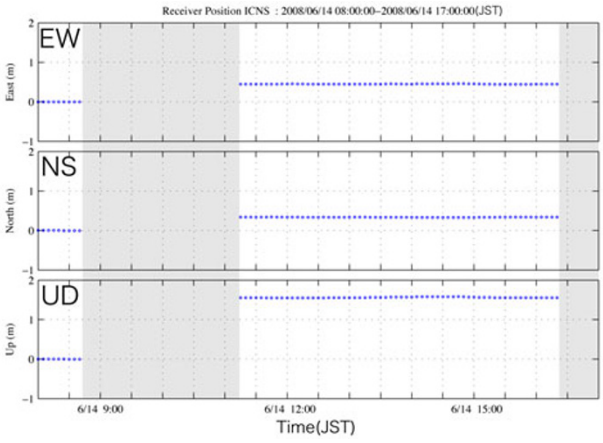


Fig. 2. Time series of coordinates at the ICNS GPS station with respect to 0154 (Iwasaki), estimated every 5 min using kinematic PPP analysis. Shadowed areas denote power outages. Notable coseismic displacements of 44 (east), 34 (north), and 156 cm (up) are clearly recorded.

Table 1. Coseismic displacements estimated by kinematic PPP analysis at each GPS station used to develop the coseismic fault model in this study. Stations were ordered in increasing longitude through the network. Some sites are located outside of the figures. TU: Tohoku University GPS network, JNES: Japan Nuclear Energy Safety Organization (JNES) GPS array, NAO: National Astronomical Observatory of Japan (NAO), GEONET: GEONET sites operated by Geographical Survey Institute (GSI).

| | Site name | Longitude (deg) | Latitude (deg) | Height (m) | de (cm) | dn (cm) | du (cm) |
|---|---|---|---|---|---|---|---|
| TU | hoj_ | 140.16798 | 39.34335 | 135.6 | 2.4 | −1.3 | 0.1 |
| | omn_ | 140.38059 | 39.28874 | 122.4 | 4.7 | −1.9 | 1.1 |
| | nnn_ | 140.39173 | 39.47618 | 72.2 | 3.7 | −2.1 | 3.6 |
| | aknm | 140.53976 | 38.95604 | 420.8 | 16.2 | −0.3 | −0.4 |
| | hrn_ | 140.62729 | 39.25821 | 182.0 | 6.1 | −4.9 | −0.2 |
| | gny_ | 140.71488 | 38.85795 | 453.2 | 28.0 | −2.2 | −0.4 |
| | iwdy | 140.86257 | 38.65338 | 123.1 | −0.5 | 0.9 | −0.7 |
| | icns | 140.86314 | 39.01206 | 468.5 | 43.9 | 33.9 | 155.7 |
| | hitg | 140.88311 | 38.85800 | 359.8 | −19.5 | 25.3 | −7.3 |
| | gto_ | 140.90800 | 39.23970 | 653.8 | 3.3 | 1.1 | 0.3 |
| | nam_ | 140.99393 | 39.46811 | 277.4 | −0.5 | 0.2 | −0.5 |
| | wyg_ | 141.11979 | 38.74221 | 59.4 | −5.9 | 3.9 | 1.4 |
| | hagn | 141.12408 | 38.86978 | 119.8 | −11.7 | 5.3 | −0.1 |
| | dit_ | 141.42169 | 39.06466 | 442.1 | −4.9 | 0.5 | −2.9 |
| | tygw | 141.42656 | 38.84869 | 214.7 | −3.9 | 1.3 | −0.8 |
| | natr | 141.55474 | 38.72233 | 66.6 | −1.6 | 1.1 | −0.8 |
| | kgj_ | 141.56144 | 39.38918 | 415.4 | 0.5 | 0.0 | 0.4 |
| | kmi_ | 141.69501 | 39.29848 | 599.8 | −1.2 | −2.0 | 2.6 |
| JNES | srhn | 140.62827 | 39.15275 | 251.5 | 14.3 | −8.2 | 1.1 |
| | isbd | 140.90437 | 39.11496 | 350.9 | 23.2 | 31.5 | 38.0 |
| | hmyo | 140.94555 | 39.11592 | 287.6 | 17.2 | 25.2 | 16.2 |
| | owky | 141.03033 | 39.12859 | 192.0 | −8.9 | 0.5 | −2.4 |
| | ntst | 141.08678 | 39.13907 | 137.1 | −8.8 | −0.7 | −1.8 |
| | otsr | 141.25388 | 39.12021 | 220.2 | −5.3 | −0.1 | 0.4 |
| | idek | 141.32259 | 39.16618 | 276.1 | −3.4 | −0.2 | 0.3 |
| NAO | mizw | 141.13282 | 39.13523 | 117.5 | −7.3 | −0.7 | 0.3 |
| | mizu | 141.13283 | 39.13517 | 117.0 | −7.2 | −1.0 | −0.8 |
| | mzsw | 141.13345 | 39.13396 | 105.7 | −8.2 | −0.4 | −0.9 |
| GEONET | 0154 | 139.92812 | 40.57764 | 48.0 | 0.0 | 0.0 | 0.0 |
| | 0192 | 140.16198 | 39.16421 | 298.4 | 3.9 | −0.8 | 2.6 |
| | 0930 | 140.18347 | 38.93810 | 174.0 | 5.0 | −0.1 | 1.4 |
| | 0927 | 140.27893 | 39.29674 | 179.7 | 2.8 | −1.7 | 0.6 |
| | 0033 | 140.31874 | 38.75860 | 181.5 | 3.4 | 0.4 | −1.8 |
| | 0929 | 140.44733 | 39.05438 | 199.8 | 10.5 | −2.3 | 0.6 |
| | 0931 | 140.49726 | 38.75216 | 236.1 | 3.6 | 0.0 | −0.1 |
| | 0554 | 140.50669 | 39.19910 | 138.6 | 7.3 | −4.0 | 0.6 |
| | 0190 | 140.55978 | 39.32700 | 104.3 | 3.2 | −2.5 | 0.3 |
| | 0193 | 140.62959 | 39.05190 | 345.0 | 27.5 | −8.6 | −2.0 |
| | 0928 | 140.71505 | 39.14620 | 322.0 | 20.5 | −13.1 | −0.1 |
| | 0544 | 140.76918 | 39.35130 | 300.9 | 2.3 | −1.3 | 0.2 |
| | 0174 | 140.80164 | 38.74894 | 343.4 | −3.2 | 1.8 | −4.4 |
| | 0913 | 140.83318 | 38.93403 | 690.7 | 93.1 | −116.6 | 209.0 |
| | 0796 | 140.98846 | 39.12701 | 228.0 | −0.8 | 2.2 | 0.0 |
| | 0173 | 140.99058 | 38.81534 | 108.5 | −13.8 | 12.6 | −0.7 |
| | 0915 | 141.00433 | 38.68613 | 105.4 | −4.0 | 3.6 | −1.1 |
| | 0912 | 141.14852 | 38.99546 | 131.7 | −13.6 | 3.1 | −0.2 |
| | 0916 | 141.16072 | 38.66063 | 51.0 | −1.9 | 2.4 | 0.2 |
| | 0029 | 141.20392 | 39.11062 | 172.1 | −7.1 | 5.1 | 1.6 |
| | 0909 | 141.29300 | 39.46469 | 244.6 | −0.4 | 0.6 | −1.5 |
| | 0910 | 141.31167 | 39.23538 | 222.4 | −2.2 | −0.3 | 0.2 |
| | 0914 | 141.31786 | 38.74322 | 58.3 | −3.7 | 2.0 | −0.7 |
| | 0911 | 141.40085 | 39.01211 | 212.2 | −4.2 | 0.4 | 0.1 |
| | 0175 | 141.44937 | 38.68270 | 84.0 | −2.0 | 1.5 | 0.1 |
| | 0169 | 141.53416 | 39.33806 | 317.0 | −0.6 | −0.3 | 0.3 |
| | 0172 | 141.57259 | 38.90286 | 82.6 | −2.6 | 0.5 | −0.3 |
| | 0546 | 141.57549 | 39.14309 | 124.8 | −1.6 | 0.0 | 0.3 |
| | 0171 | 141.73985 | 39.02378 | 106.8 | −0.7 | 0.0 | 0.7 |

seismic displacements, which were obtained by integrating the accelerogram at the Ichinoseki-nishi seismic station, which was located 200 m away from the ICNS GPS station. NIED found displacements of 45 cm east, 44 cm north, and 140 cm up (NIED, 2008). Integrated seismogram records are possibly contaminated by biases during the integral operation, which may degrade the signal-to-noise ratio. Within this context, the fact that these two independent data sets show approximately the same coseismic displacements suggests that the displacements observed are independent of instrument type and are caused by actual ground motion associated with the mainshock.

### 3.2 Fault model of the mainshock

A detailed aftershock distribution was obtained by the dense temporal aftershock observation network. This temporal seismic network is operated by group for the aftershock observations of the Iwate-Miyagi Nairiku earthquake in 2008 (GIMNE2008, hereafter). GIMNE2008 (2008) determined the precise aftershock distribution using the double-difference hypocenter determination technique (Zhang and Thurber, 2003) to reveal a coseismic fault dipping west-northwestward in the northern part of the focal

Table 2. Model fault parameters consisting of two rectangular faults. Longitude, latitude, and depth denote the location of the upper-left corner of each rectangular fault plane, looking down from the hanging wall side.

| Fault plane | Longitude (degree) | Latitude (degree) | Depth (km) | Length (km) | Width (km) | Strike (degree) | Dip (degree) | Rake (degree) | Slip (m) |
|---|---|---|---|---|---|---|---|---|---|
| North | 140.979 | 39.109 | 0.46 | 20.57 | 12.06 | 195.2 | 44.9 | 105.5 | 1.83 |
| South | 140.907 | 38.927 | 0.40 | 12.57 | 10.10 | 225.3 | 25.0 | 80.9 | 3.53 |

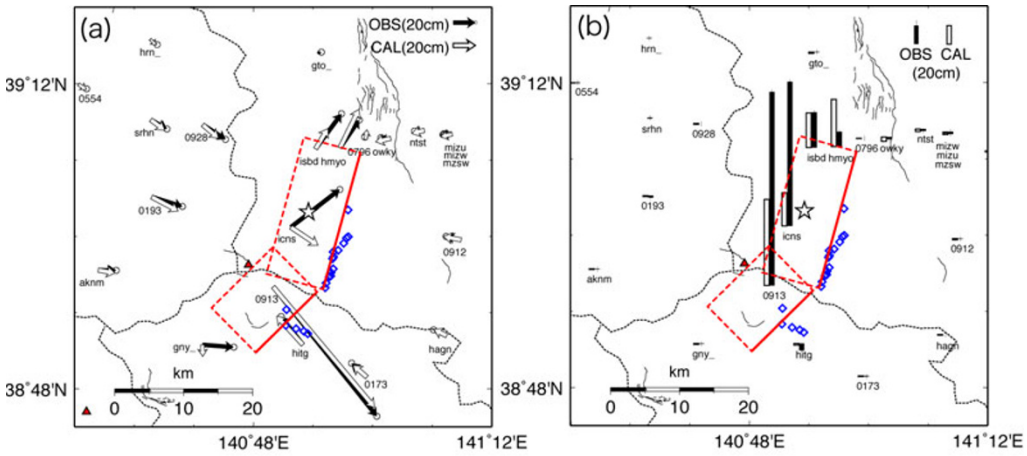


Fig. 3. Comparisons between observed and calculated coseismic displacements. (a) Horizontal displacements and (b) vertical displacements. Black arrows and bars denote observed displacements caused by the IMEQ main shock with their associated error ellipses. White arrows and bars indicate calculated displacements from the estimated fault model. The model fault geometry is shown by the red rectangles with broken and solid lines indicating the lower and upper edges of the faults, respectively. The blue diamonds denote significant surface ruptures and deformations found by AIST (2008). The red triangle represents Mt. Kurikoma. The white star denotes the mainshock epicenter.

area. In contrast, the southern part shows a slightly lower dip angle relative to that of the northern part (Fig. 1). The National Institute of Advanced Industrial Science and Technology of Japan (AIST) (2008) found significant surface ruptures and deformation based on field surveys. These surface ruptures were formed coseismically and are characteristic in thrust faulting around the eastern edge of the focal area (Fig. 3). These observations also suggest that coseismic fault motion generates ground rupture and deformation. Based on the aftershock distribution and surface deformations, we assume that the W-NW dipping fault planes also apply for the coseismic deformations. The rectangular fault parameters in an elastic half space (Okada, 1992) were estimated by inversion analysis with a priori information. It is well known that inversion results depend on a priori information. We constrained the fault plane location (latitude and longitude, 0.01° limitation to change), length (5 km limitation), and dip angle (5°) for the inversion analysis, and we changed the initial value by trial and error process.

The estimated fault parameters are listed in Table 2. Our very simple model explains the data well and reproduces the complex spatial pattern, especially in the northern part of the focal area (Fig. 3). The vertical component also basically successfully reproduces the observed one. At the ICNS station, however, the model fails to explain the NW horizontal displacement, and the vertical component of 0913 and the ICNS station are not consistent with the observed one. These discrepancies may have been caused by slip heterogeneity along the fault. The estimated seismic moment of the mainshock was $2.70\times10^{19}$ N m, which corresponds to $M_w$ 6.9. The coseismic slip reaches 3.5 m on

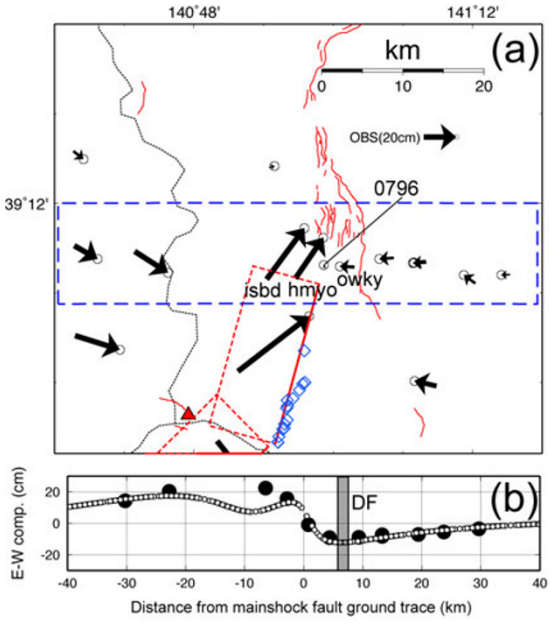


Fig. 4. (a) GPS displacements identified in Fig. 3. The red diamonds denote significant surface ruptures and deformations found by AIST (2008). Red rectangles denote the coseismic fault model. The dashed blue rectangle denotes the approximately area of the E-W displacement profiles shown in (b). Red triangles represent Mt. Kurikoma. (b) The E-W profile of eastward displacements. Solid circles represent observed displacements at each GPS station. Open circles represent calculated displacements from the coseismic fault model. Shadow belts denote the surface trace of the DF.

the southern fault, but on the northern fault, it is less than 2 m.

### 3.3 Relationship between the Dedana fault and the mainshock

The JNES sites provide a strong constraint for estimating the coseismic fault parameters. It is clear that the HMYO (JNES) and ISBD (JNES) stations are located on the hanging wall side and near the edge of the fault plane because of the horizontal displacement vectors showing NE displacements. In contrast, OWKY (JNES) and 0796 (GEONET) are located on the footwall sides of the fault plane because of the horizontal vectors directed north-northwest with small displacements (Fig. 3(a), 4). Figure 4(b) compares the observed eastward displacements with the theoretical ones calculated from our fault model. The location of the upper edge of the model fault is obviously different from the surface trace of the Dedana fault. The GPS data suggest that the upper edge of the coseismic fault is located several kilometers west of the surface trace of the Dedana fault (Fig. 4). The estimated depth of the northern part's upper edge is less than 1 km (Table 2). We can therefore conclude that IMEQ occurred on an unidentified fault system, and not that of the Dedana fault. This result has provided an important constraint for investigating the process of strain accumulation around the Dedana fault.

## 4. Conclusion

We propose a coseismic fault model for the 2008 Iwate-Miyagi Nairiku earthquake ($M_j$ 7.2) deduced using data from a dense GPS network. The coseismic displacements were estimated by the PPP kinematic approach. The results indicate that a simple rectangular fault model could explain observations, except for the data at the ICNS station, probably because of heterogeneity in the slip distribution. The amount of moment release was estimated to be $M_w$ 6.9. The coseismic slip reached 3.5 m on the southern fault. Based on the GPS data, we conclude that the coseismic slip of the mainshock did not occur on the Dedana fault system.

**Acknowledgments.** We thank the Group for the aftershock observations of the Iwate-Miyagi Nairiku Earthquake in 2008 (GIMNE2008) for providing the precise catalog of aftershocks. The paper benefited from careful reviews by Prof. Takao Tabei and Dr. Andria Bilich. This study is based on GPS data obtained by the investigation project conducted by Japan Nuclear Energy Safety Organization (JNES) to establish evaluation techniques of seismogenic faults. We thank GSI and NAO for providing GPS data. We thank Mr. T. Takasu for providing us his GPS analysis codes called "GpsTools ver. 0.6.3". This study is partly supported by a Grant-in-Aid for Young Scientists (Start-up: No. 19840006) Research of Japan Society for the Promotion of Science. Figures were drawn using GMT software (Wessel and Smith, 1991).

## References

Advanced Industrial Science and Technology, the headquarters for Earthquake Research Promotion, 11 July 2008, 2008 (in Japanese with an English abstract).

Dow, J., R. Neilan, and G. Gendt, The international GPS service (IGS): celebrating the 10th anniversary and looking to the next decade, *Adv. Space Res.*, **36**(3), 320–326, 2005.

Group for the aftershock observations of the Iwate-Miyagi Nairiku Earthquake in 2008 (GIMNE2008), the headquarters for Earthquake Research Promotion, 24 July 2008, 2008 (in Japanese with an English abstract).

Hasegawa, T., S. Hori, T. Hasegawa, K. Kasahara, S. Horiuchi, and J. Koyama, On the focal mechanism of the Southeastern Akita Earthquake in 1970, *J. Seismol. Soc. Jpn.*, **27**, 302–312, 1974 (in Japanese with an English abstract).

Hasegawa, A., K. Kasahara, T. Hasegawa, and S. Hori, On the focal mechanism of the Southeastern Akita Earthquake in 1970 (2), *J. Seismol. Soc. Jpn.*, **28**, 141–151, 1975 (in Japanese with an English abstract).

Hatanaka, Y., Improvement of the Analysis Strategy of GEONET, *Bull. Geogr. Surv. Inst.*, **49**, March, 2003.

Kouba, J., Measuring seismic waves induced by large earthquakes with GPS, *Stud. Geophys. Geodyn.*, **47**(4), 741–755, 2003.

Larson, K., P. Bodin, and J. Gomberg, Using 1-Hz GPS Data to Measure Deformations Caused by the Denali Fault Earthquake, *Science*, **300**, 30 May, 2003.

Matsuda, T., H. Yamazaki, T. Nakata, and T. Imaizumi, The surface faulting associated with Riku-u earthquake of 1896, *Bull. Earthq. Res. Inst. Tokyo Univ.*, **55**, 795–855, 1980 (in Japanese with an English abstract).

Miura, S., S. Ueki, T. Sato, K. Tachibana, and H. Hamaguchi, Crustal deformation associated with the 1998 seismo-volcanic crisis of Iwate Volcano, Northeastern Japan, as observed by a dense GPS network, *Earth Planets Space*, **52**, 1003–1008, 2000.

Miura, S., T. Sato, K. Tachibana, Y. Satake, and A. Hasegawa, Strain accumulation in and around Ou Backbone range, northeastern Japan as obsered by a dense GPS network, *Earth Planets Space*, **54**, 1071–1076, 2002.

Miura, S., T. Sato, A. Hasegawa, Y. Suwa, K. Tachibana, and S. Yui, Strain concentration zone along the volcanic front derived by GPS observations in NE Japan arc, *Earth Planets Space*, **56**, 1347–1355, 2004.

Miura, S., T. Iinuma, S. Yui, N. Uchida, T. Sato, K. Tachibana, and A. Hasegawa, Co- and post-seismic slip associated with the 2005 Miyagi-oki earthquake (M7.2) as inferred from GPS data, *Earth Planets Space*, **58**, 1567–1572, 2006.

Miyazaki, S. and K. M. Larson, Coseismic and early postseismic slip for the 2003 Tokachi-oki earthquake sequence inferred from GPS data, *Geophys. Res. Lett.*, **35**, L04302, doi:10.1029/2007GL032309, 2008.

NIED, http://www.hinet.bosai.go.jp/topics/iwate-miyagi080614/, 2008.

Okada, Y., Internal deformation due to shear and tensile faults in a halfspace, *Bull. Seismol. Soc. Am.*, **82**, 1018–1040, 1992.

Ohta, Y., I. Meilano, T. Sagiya, F. Kimata, and K. Hirahara, Large surface wave of the 2004 Sumatra-Andaman earthquake captured by the very long baseline kinematic analysis of 1-Hz GPS data, *Earth Planets Space*, **58**, 153–157, 2006.

Takasu, T., High-rate Precise Point Positioning: Detection of crustal deformation by using 1-Hz GPS data, *GPS/GNSS Symposium 2006*, Tokyo, 2006.

Takasu, T. and S. Kasai, Development of Precise Orbit/Clock Determination Software for GPS/GNSS, *the 49th Space Sciences and Technology Conference*, Hiroshima, Japan, 2005.

Umino, N., T. Okada, A. Nakamura, J. Nakajima, T. Sato, S. Hori, T. Kono, K. Nida, S. Ueki, T. Matsuzawa, A. Hasegawa, and H. Hamaguchi, Aftershock distribution for the M6.1 earthquake of 3 September 1998 in Shizukuishi, Iwate prefecture, northeastern Japan, *Active Fault Res.*, **17**, 1–8, 1998 (in Japanese with an English abstract).

Wessel, P. and W. H. F. Smith, Free software helps map and display data, *EOS Trans. AGU*, **72**, 445–446, 1991.

Zhang, H. J. and C. H. Thurber, Double-difference tomography: the method and its application to the Hayward fault, California, *Bull. Seism. Soc. Am.*, **93**, 1875–1889, 2003.

Zumberge, J. F., M. B. Heflin, D. C. Jefferson, M. M. Watkins, and F. H. Webb, Precise point positioning for the efficient and robust analysis of GPS data from large networks, *J. Geophys. Res.*, **102**(B3), 5005–5017 MAR 10, 1997.

Y. Ohta (e-mail: ohta@aob.geophys.tohoku.ac.jp), M. Ohzono, S. Miura, T. Iinuma, K. Tachibana, K. Takatsuka, K. Miyao, T. Sato, and N. Umino